Engineering bound states in continuum via a nonlinearity-induced extra dimension

Qingtian Miao,[1,2,*] Jayakrishnan M. P. Nair,[1,2,†] and Girish S. Agarwal[1,2,3,‡]

[1]*Institute for Quantum Science and Engineering, Texas A&M University, College Station, Texas 77843, USA*
[2]*Department of Physics and Astronomy, Texas A&M University, College Station, Texas 77843, USA*
[3]*Department of Biological and Agricultural Engineering, Texas A&M University, College Station, Texas 77843, USA*

(Received 3 July 2023; revised 2 September 2023; accepted 4 October 2023; published 17 October 2023)

Bound states in continuum (BICs) are states of a system possessing significantly large lifetimes with applications across various branches of science. In this work, we propose an expedient protocol to engineer BICs using the Kerr nonlinearities of a system which otherwise has no BICs. The generation of BICs is a direct artifact of the nonlinearity and the associated expansion in the dimensionality of the system. In particular, we consider single- and two-mode anharmonic systems and provide a number of solutions apposite for the creation of BICs. The nonlinearity-induced BICs can be controlled by external drive. In close vicinity to the BIC, the steady state response of the system is immensely sensitive to perturbations in natural frequencies of the system, and we illustrate its propitious sensing potential in the context of experimentally realizable setups for both optical and magnetic nonlinearities.

DOI: 10.1103/PhysRevResearch.5.043053

I. INTRODUCTION

The localization of electromagnetic waves has been a subject of intense research over the past few decades [1]. It is well known that the solutions of the Schrödinger equation below the continuum threshold possess discrete energies and are square integrable in nature. In contrast, above the continuum threshold, energy eigenvalues are continuous and the solutions are unbounded. However, it has been shown that there exist localized states within the continuum of energies, namely the bound states in continuum. BICs were first proposed in 1929 by von Neumann and Wigner [2] in an electronic system and Stillinger and Herrick later extended it to a two-electron wave function [3]. However, the first experimental observation of BICs came only in 1992 by Capasso *et al.*, who demonstrated an electronic bound state in a semiconductor superlattice [4].

The emergence of BICs in electromagnetic systems can be explicated by investigating the effective non-Hermitian Hamiltonian ensuing from the Maxwell's equations, resulting in complex resonance frequencies ω. BICs are, in essence, nonradiating solutions of the wave equations, i.e., modes of the system with $\mathrm{Im}(\omega)$ approaching zero. In the last decade, BICs have been realized in a multitude of settings involving, for example, electronic [5–7], acoustic [8–10], and photonic [11] subsystems. In particular, owing to their excellent tunability, photonic systems have emerged as an excellent candidate in recent years with applications including, but not limited to, the design of high-Q resonators [12–14], lasing [15–22], sensing [23–32], filters [33,34], etc. In [24], Romano *et al.* reported an optical sensor underpinned by BIC for the fine grained estimation of perturbations in a dielectric environment. Another recent work [25] reported the development of nanophotonic sensor based on high-Q metasurface elements for molecular detection with applications in biological and environmental sensing. Some other recent intriguing research topics include the enhanced sensing of spontaneous emission [27], vortex generation [35,36], switches [37], efficient higher harmonic generation [38,39], and many more.

In this paper, we propose Kerr nonlinearities as a resource to engineer BICs in systems which do not possess BICs in the absence of nonlinearities. Such nonlinearities can be observed in a plentitude of physical systems ranging from optical cavities [40] to magnetic systems [41], and have been a subject of prime interest, with many exotic effects [42–45]. Here, we present a variety of solutions for BICs relevant to single- and two-mode bosonic systems having a Kerr type of anharmonicity. The resulting BICs are strongly sensitive to perturbations in the system parameters, in particular variations in characteristic detunings which owe their origin to the existence of first- and second-order poles in the response function. In addition, we discuss a number of experimental platforms germane to our analysis of the nonlinear systems. In particular, we specifically illustrate the sensing capabilities of BICs in two-mode anharmonic systems which are experimentally realizable. The sensing at BIC does not require gain in the system, which is different from sensing at exception points [46,47].

The paper is organized as follows. In Sec. II, we discuss the well known schemes for the generation of BICs without involving the use of Kerr nonlinearities. Subsequently, in Sec. III, we provide a detailed analysis of the protocol

*qm8@tamu.edu
†jayakrishnan00213@tamu.edu
‡girish.agarwal@ag.tamu.edu

to achieve BICs in a single-mode system with passive Kerr nonlinearity and the accompanying sensitivity to perturbations in the system. We extend the study into the domain of a two-mode active nonlinear system in Sec. IV and establish its equivalence with the single-mode results in the Appendix. Finally, we conclude our results in Sec. V.

II. BIC IN A COUPLED TWO-MODE SYSTEM

We commence our analysis by revisiting the emergence of BICs in a generic two-mode system without any nonlinearities. To this end, we consider a system comprising modes a and b coupled through a complex parameter J and driven externally at frequency ω_d. The dynamics of the system in the rotating frame of the drive is given by

$$\dot{X} = -i\mathcal{H}X + F_{in}, \tag{1}$$

where, $X^T = [a\ b]$, F_{in} describes the modality of external driving and $\mathcal{H}$ is the effective non-Hermitian Hamiltonian provided by

$$\mathcal{H} = \begin{pmatrix} \Delta_a - i\kappa & J \\ J & \Delta_b - i\gamma \end{pmatrix}. \tag{2}$$

Here, $\Delta_i = \omega_i - \omega_d$ where $i \in \{a, b\}$, ω_a and ω_b are the characteristic resonance frequencies of the modes a and b, and κ, γ denote their respective decay rates. Note that the real and imaginary parts of $J = g - i\Gamma$ represent the coherent and dissipative form of coupling between the modes. The eigenvalues of $\mathcal{H}$ are given by $\lambda_\pm = \frac{\Delta_a+\Delta_b}{2} - i\bar{\gamma} \pm \sqrt{(\frac{\Delta_a-\Delta_b}{2} - i\tilde{\gamma})^2 + (g - i\Gamma)^2}$, where $\bar{\gamma} = \frac{\kappa+\gamma}{2}$ and $\tilde{\gamma} = \frac{\kappa-\gamma}{2}$. One of the ways to bring to naught the imaginary part of the eigenvalues is to employ engineered gain into the system, that is to make $\kappa = -\gamma$. This in conjunction with the absence of dissipative coupling, viz., $\Gamma = 0$ and $\Delta_a = \Delta_b$ yield the eigenvalues $\lambda_\pm = \Delta_a \pm \sqrt{(g^2 - \gamma^2)}$. Palpably, the system in the parameter domain $g \geqslant \gamma$ is earmarked by the observation of real eigenspectra [48]. Note that the system under this parameter choice lends itself to a PT-symmetric description of the effective Hamiltonian featuring an exceptional point (EP) in the parameter space at $g = \gamma$. On the other hand, the region $g < \gamma$ affords eigenvalues which form a complex-conjugate pair, wherein the amplitude of the modes grows exponentially in time whereas the other one decays. In the context of PT-symmetric systems, it is important to notice that EPs, which have found applications in sensing [46,47], are functionally analogous to BICs.

There exists another interesting parameter domain, conformable with anti-PT symmetry, i.e., $\{PT, \mathcal{H}\} = 0$, that can spawn a BIC, without involving external gain. Such a system necessitates the absence of coherent coupling, that is to say $g = 0$, $\kappa = \gamma$, and $\Delta_a = -\Delta_b$, begetting $\lambda_\pm = -i\kappa \pm \sqrt{(\Delta_a^2 - \Gamma^2)}$, which take purely imaginary form when $|\Delta_a| \leqslant \Gamma$. In contrast, the $|\Delta_a| > \Gamma$ phase leads to decaying solutions with real parts of the eigenvalues lying on either side of the external drive frequency. Observe that when $\Delta_a = 0$ and as Γ approaches κ, the system entails a BIC, marked by the existence of a vanishing eigenvalue, i.e., $\lambda_+ \to 0$, and thereby eliciting a pole at origin in response to the external drive. The anti-PT symmetric system does not warrant the use of gain; however, it stipulates the use of dissipative coupling, which can be engineered by coupling the subsystems via a common intermediary reservoir [45,49–51].

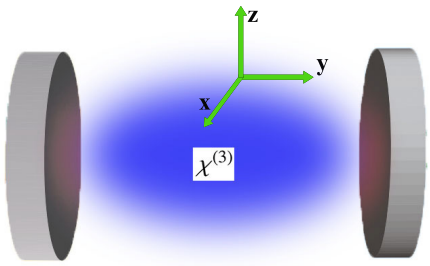

FIG. 1. A third-order Kerr nonlinear medium in an optical cavity.

It makes for a relevant observation that, in general, the effective Hamiltonian in Eq. (1) does not yield nonradiating solutions of the Maxwell equations, especially when $J = 0$, i.e., when the modes are decoupled. In the following section, we provide a mechanism to engineer BIC in a nonlinear system, which in the absence of nonlinearity has no BICs. An example of a linear system with no BIC would be the Hamiltonian $\mathcal{H}$ in Eq. (2) with J real and no gain, i.e., $\kappa, \gamma > 0$. In fact, the existence of BIC is an inalienable consequence of anharmonicities present in the system and the concomitant magnification of the dimensionality. The mechanism can be extended to two-mode nonlinear systems, and we provide a detailed analysis with explicit examples in Sec. IV.

III. BIC IN A SINGLE-MODE KERR NONLINEAR SYSTEM

We consider a medium with third-order Kerr nonlinearity characterized by a nonlinear contribution to the polarization $P^{(3)}(\omega) = \chi^{(3)}|E(\omega)|^2 E(\omega)$ placed in a single-mode cavity with mode variable a as depicted in Fig. 1. Here, E is the cavity electric field and $\chi^{(3)}$ the third-order nonlinear susceptibility. The cavity is driven externally from the left at frequency ω_d with a field strength proportional to $\mathcal{E}$. The passive nature of nonlinearity indicates that the nonlinear processes are only affected by the frequency composition of the field and not the medium, which only plays a catalytic role [52]. The dynamics of the system in the rotating frame of the drive is given by

$$\dot{a} = -(i\Delta + \gamma)a - i2U|a|^2 a + \mathcal{E}, \tag{3}$$

where $\Delta = \omega_a - \omega_d$, ω_a denotes the cavity resonance frequency, $U = \frac{3\hbar\omega_a^2\chi^{(3)}}{4\epsilon_0 n V_{\text{eff}}}$ is a measure of Kerr nonlinearity of the medium with refractive index n, V_{eff} signifies the effective volume of the cavity mode having a leakage rate γ, and $\mathcal{E} = \sqrt{\frac{2\gamma P_d}{\hbar\omega_d}}$ represents the Rabi frequency of external driving. In the long-time limit, the mode a decays into a steady state described by the cubic equation

$$I = \frac{\alpha}{2}\left[1 + \left(\tilde{\Delta} + \frac{\alpha}{2}\right)^2\right], \tag{4}$$

where $I = \frac{2U|\mathcal{E}|^2}{\gamma^3}$, $\alpha = 4\frac{U}{\gamma}|a_0|^2$, $\tilde{\Delta} = \Delta/\gamma$, and a_0 is the steady amplitude of the mode a. The output intensity is proportional to α. The Eq. (4) can engender a bistable response

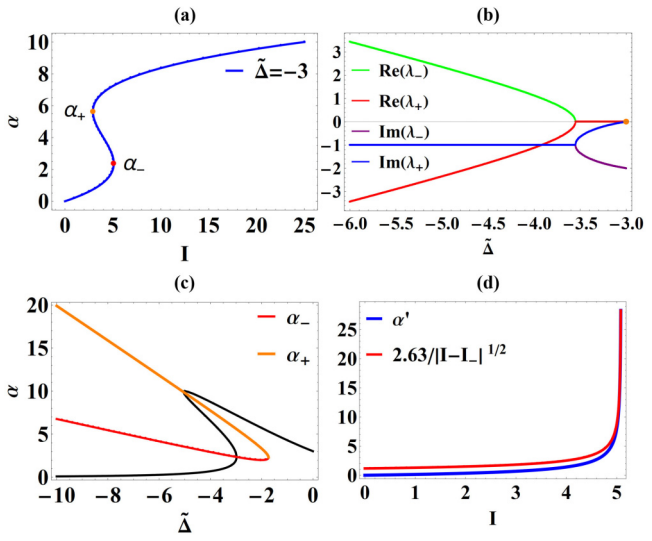

FIG. 2. (a) The I-α curve, given by Eq. (4), for the single mode Kerr nonlinear system when $\tilde{\Delta} = -3$. The turning points $\alpha_\pm$ [Eq. (5)] are as denoted in the figure. (b) The real and imaginary parts of the eigenvalues of $\mathcal{H}$ as a function of $\tilde{\Delta}$ for $\alpha = 2.367$. The orange point indicates BIC. (c) The $\tilde{\Delta}$-α curve given by Eq. (4) for input $I = 5$ (black line) and the turning points $\alpha_\pm$ [Eq. (5)] plotted against $\tilde{\Delta}$ (orange line and red line, respectively). (d) $\alpha' = \frac{d\alpha}{d\tilde{\Delta}}$ and $2.63/|I - I_-|^{1/2}$ are plotted against I to make a comparison when $\tilde{\Delta} = -3$.

under the condition $U\Delta < 0$ and $\Delta^2 > 3\gamma^2$ as illustrated by Fig. 2(a). Notably, there exist two turning points characterized by the coordinates $(I_\pm, \alpha_\pm)$ of the I-α curve, subject to $\frac{dI}{d\alpha} = 0$, beyond which we observe an abrupt change in α. The exact form of $\alpha_\pm$ is given by

$$\alpha_\pm = \frac{-4\tilde{\Delta} \pm 2\sqrt{\tilde{\Delta}^2 - 3}}{3}, \tag{5}$$

while $I\pm$ can be obtained from Eq. (4) by substituting the above-mentioned solutions. Moreover, there is a cutoff for the pump power beyond which the bistable characteristics set in. The critical magnitude of I^c is defined by the inflection point in the I-α graph described by the condition $\frac{dI}{d\alpha} = \frac{d^2I}{d\alpha^2} = 0$, providing us

$$I^c = -\frac{\alpha^2}{2}\left(\tilde{\Delta} + \frac{\alpha}{2}\right). \tag{6}$$

For a given set of parameters U, I, Δ, and γ, we would like to perturb the system in Δ, modifying the mode variable into $a = a_0 + \delta a$, in which δa characterizes the perturbations of the mode a about a_0. The dynamics of the perturbations are governed by the following effective Hamiltonian:

$$\tilde{\mathcal{H}} = \begin{pmatrix} \tilde{\Delta} + \alpha - i & \beta \\ -\beta^* & -\tilde{\Delta} - \alpha - i \end{pmatrix}, \tag{7}$$

where $\beta = \frac{2U}{\gamma}a_0^2$. The complex eigenvalues of the Eq. (7) denoted as λ refer to the normal modes of the system and they can be obtained by solving the characteristic polynomial equation

$$\lambda^2 + 2i\lambda + |\beta|^2 - (\tilde{\Delta} + \alpha)^2 - 1 = 0. \tag{8}$$

Notably, in the limit when the determinant of the Hamiltonian

$$\left(\frac{\alpha}{2}\right)^2 - (\tilde{\Delta} + \alpha)^2 - 1 \to 0, \tag{9}$$

one of the solutions of Eq. (8) becomes vanishingly small. Note that we are working in the frame rotating at frequency ω_d. Therefore, under this condition, the imaginary part of one of the eigenvalues approaches zero, alluding to the generation of a BIC, as depicted in Fig. 2(b). It is worth noting that $\alpha \neq 0$, i.e., $U \neq 0$, is a prerequisite for the existence of such a state. In other words, the generated BIC owes its origin entirely to the Kerr anharmonicities of the mode a. For a given value of the parameter Δ, the BICs exist at $(I_\pm, \alpha_\pm)$, which are exactly the turning points of the I-α curve as depicted in Figs. 2(a) and 2(c). It has to be kept in mind that if for experimental reasons it is not easy to reach exactly the BIC point, then the response would depend on $\mathrm{Im}(\lambda_+)$, whose value can be read off from Fig. 2(b). Since in such a case $\mathrm{Im}(\lambda_+) \neq 0$, one can call such points as quasibound states.

Application of nonlinearity-induced BIC in sensing. The existence of BICs also leads to the enhanced sensitivity of the nonlinear response to perturbations in the system parameters. This can be accredited to the existence of the first- and second-order poles at $\alpha = \alpha_\pm$ in the first-order derivative of the nonlinear response,

$$\frac{d\alpha}{d\tilde{\Delta}} = -\frac{8\alpha(\tilde{\Delta} + \alpha/2)}{3(\alpha - \alpha_-)(\alpha - \alpha_+)}, \tag{10}$$

obtained from differentiating Eq. (4) by $\tilde{\Delta}$. To further elucidate the origin of sensitivity, we expand I around the turning points of the I-α curve, that is, around $\alpha = \alpha_\pm$, $I = I_\pm + \frac{\partial I}{\partial \alpha}\epsilon + \frac{\partial^2 I}{\partial \alpha^2}\epsilon^2 + O(\epsilon^3)$, where $\epsilon = \alpha - \alpha_\pm$ and $I_\pm$ are obtained by substituting $\alpha_\pm$ in Eq. (4). Consequently, at the turning points of the curve, $\frac{\partial I}{\partial \alpha} = 0$ and we have $|\frac{d\alpha}{d\tilde{\Delta}}| \sim |I - I_\pm|^{-1/2}$. On the other hand, close to inflection point sensitivity has the functional dependence $|\frac{d\alpha}{d\tilde{\Delta}}| \sim |I - I_c|^{-2/3}$. In practice, one can choose a value of $\tilde{\Delta}$ and Eq. (9) in conjunction with Eq. (4) to determine the corresponding $\alpha_\pm$ and $I_\pm$ appropriate for sensing. As I is varied tantalizingly close to $I_\pm$, any perturbations in the parameter Δ translate into a prodigious shift in the mode response, as is perceptible from Fig. 2(d). Note that the sensitivity to aberrations in Δ is a direct artifact of the existence of a BIC.

Bearing in mind the generality of our analysis, it is interesting to observe the variety of experimental platforms available to implement our scheme for investigating BICs produced by nonlinearity-induced extra dimensions. Some of the well-known examples in the context of passive nonlinearities and bistability include sodium vapor [53], ruby [54], Kerr liquids like CS_2, nitrobenzene, electronic nonlinearity of Rb vapor, etc., to name a few [40,55]. In the subsequent section, we stretch the analysis into the case of two-mode anharmonic, systems which are ubiquitous in nature.

IV. ENGINEERING BIC IN A TWO-MODE KERR NONLINEAR SYSTEM

We begin this section by considering a two-mode active Kerr nonlinear system that consists of modes a and b coupled coherently through a real parameter g, and b is externally

pumped at a frequency of ω_d. The Hamiltonian of the system can be expressed as

$$H/\hbar = \omega_a a^\dagger a + \omega_b b^\dagger b + g(b^\dagger a + b a^\dagger) + U b^\dagger b b^\dagger b + i\Omega(b^\dagger e^{-i\omega_d t} - b e^{i\omega_d t}), \quad (11)$$

where ω_a and ω_b represent the resonance frequencies of the modes a and b, the coefficient U quantifies the strength of Kerr nonlinearity, and Ω denotes the Rabi frequency of the external field driving the b mode. The systems characterized by the aforementioned Hamiltonian are prevalent in nature, for example, a collection of two-level atoms under the conditions of no saturation which act as an active Kerr nonlinear medium in a driven resonant cavity. The dynamics of the system in the rotating frame of the drive is provided by

$$\dot{a} = -(i\delta_a + \gamma_a)a - igb,$$
$$\dot{b} = -(i\delta_b + \gamma_b)b - 2iUb^\dagger bb - iga + \Omega, \quad (12)$$

where $\delta_a = \omega_a - \omega_d$, $\delta_b = \omega_b + U - \omega_d$, and γ_a and γ_b denote the dissipation rates of the modes a and b, respectively. In the long-time limit, the system decay into a steady state, i.e., $a \to a_0$, $b \to b_0$, giving the following nonlinear cubic equation:

$$I = 4x^3 + 4\tilde{\delta}_R x^2 + |\tilde{\delta}|^2 x, \quad (13)$$

where $I = U\Omega^2$, $x = U|b_0|^2$, $\tilde{\delta} = \delta_b - i\gamma_b - \frac{g^2}{\delta_a - i\gamma_a}$, and we define $\tilde{\delta}_R = \delta_b - \frac{g^2\delta_a}{\delta_a^2+\gamma_a^2}$ and $\tilde{\delta}_I = -\gamma_b - \frac{g^2\gamma_a}{\delta_a^2+\gamma_a^2}$ as the real and imaginary parts of $\tilde{\delta}$, respectively. Notice that $\tilde{\delta}_I$ is negative. Under the criterion $\tilde{\delta}_R < \sqrt{3}\tilde{\delta}_I$, there exist three possible roots for x, leading to a bistable response, wherein two of the roots are stable while the third is unstable. The output intensity from the cavity is proportional to x.

Conditions for the existence of BIC. To analyze the effect of perturbations around the steady state, we use a linearized approximation by letting $a = a_0 + \mathscr{A}$ and $b = b_0 + \mathscr{B}$, where $\mathscr{A}$ and $\mathscr{B}$ signify the perturbations of mode a about a_0 and mode b about b_0, respectively. The dynamics of the perutrbations $\psi^T = [\mathscr{A}, \mathscr{B}, \mathscr{A}^\dagger, \mathscr{B}^\dagger]$ are governed by the following equation:

$$\frac{\partial \psi}{\partial t} = -i\mathcal{H}\psi + \mathcal{I}, \quad (14)$$

where $\mathcal{H}$ is the effective Hamiltonian

$$\mathcal{H} = \begin{pmatrix} \delta_a - i\gamma_a & g & 0 & 0 \\ g & \delta_b + 4x - i\gamma_b & 0 & 2Ub_0^2 \\ 0 & 0 & -\delta_a - i\gamma_a & -g \\ 0 & -2Ub_0^{*2} & -g & -\delta_b + 4x - i\gamma_b \end{pmatrix}, \quad (15)$$

and $\mathcal{I} = 0$ for the steady state. The normal modes of the system are hallmarked by complex eigenvalues of Eq. (15), which can be obtained by solving the characteristic polynomial equation $\det(\mathcal{H} - \lambda\mathbf{I}) = 0$. Conspicuously, when $\det\mathcal{H} = 0$, one of the eigenvalues can approach zero (in the rotating frame of the drive), spawning real eigenvalues and thereby indicating the emergence of a BIC. Therefore, we first determine the parameter domain consistent with condition

$$0 = \det\mathcal{H} = 12\left(\delta_a^2 + \gamma_a^2\right)x^2 + 8\left(-\delta_a g^2 + \delta_b\delta_a^2 + \delta_b\gamma_a^2\right)x + (g^2 - \delta_a\delta_b + \gamma_a\gamma_b)^2 + (\delta_a\gamma_b + \delta_b\gamma_a)^2. \quad (16)$$

It is worth noting that the existence of BIC relies on the prerequisite $x = U|b_0|^2 \neq 0$. In other words, the Kerr anharmonicities of the mode b are solely responsible for the creation of the BIC. Upon solving Eq. (16), we discover that BICs can exist at points

$$x_\pm = -\tfrac{1}{3}\tilde{\delta}_R \pm \tfrac{1}{6}\sqrt{\tilde{\delta}_R^2 - 3\tilde{\delta}_I^2}, \quad (17)$$

which are exactly the turning points of the I-x curve given in Eq. (13), obtained from solving the condition $\frac{dI}{dx} = 0$.

While invoking the linearized dynamics, one must make sure that the dynamical system is stable, which is to ensure that the eigenvalues of $\mathcal{H}$ have negative imaginary parts. Consequently, we define λ_R and λ_I as the real and imaginary parts of the complex eigenvalues, respectively, and let $\lambda' = -i\lambda$. The characteristic polynomial equation can then be written as

$$0 = \det(\mathcal{H} - i\lambda'\mathbf{I}) = \lambda'^4 + a_1\lambda'^3 + a_2\lambda'^2 + a_3\lambda' + a_4, \quad (18)$$

where

$$a_1 = 2(\gamma_a + \gamma_b), \quad a_2 = \delta_a^2 + 2g^2 + \left(\gamma_a^2 + 4\gamma_a\gamma_b + \gamma_b^2\right) + \left(12x^2 + 8\delta_b x + \delta_b^2\right),$$
$$a_3 = 2\delta_a^2\gamma_b + 2\delta_b^2\gamma_a + 2(\gamma_a\gamma_b + g^2)(\gamma_a + \gamma_b) + 16\delta_b\gamma_a x + 24\gamma_a x^2, \quad a_4 = \det\mathcal{H}. \quad (19)$$

The stability conditions of the system can be obtained by employing the Routh-Hurwitz criteria, yielding the constraints $a_1 > 0$, $a_3 > 0$, $a_4 > 0$, and $a_1a_2a_3 > a_3^2 + a_1^2a_4$. Apparently, the first two conditions are met automatically, and we find

$$a_1a_2a_3 - a_3^2 - a_1^2a_4 = 4\gamma_a\gamma_b\left(12x^2 + 8\delta_b x - \delta_a^2 + \delta_b^2\right)^2 + 4\gamma_a\gamma_b(\gamma_a + \gamma_b)^2\left[24x^2 + 16\delta_b x + 2\left(\delta_a^2 + \delta_b^2\right) + (\gamma_a + \gamma_b)^2\right] + 4g^2(\gamma_a + \gamma_b)^2[12x^2 + 8(\delta_a + \delta_b)x + (\delta_a + \delta_b)^2 + (\gamma_a + \gamma_b)^2], \quad (20)$$

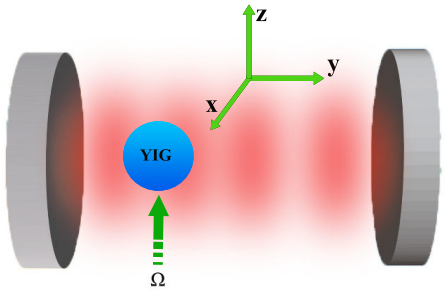

FIG. 3. Schematic of the cavity-magnon system.

which is manifestly positive, fulfilling the final criterion. The only remaining criterion $a_4 = \det \mathcal{H} > 0$ is satisfied along with $\tilde{\delta}_R < \sqrt{3}\tilde{\delta}_I$ and $x \in (0, x_-) \cup (x_+, \infty)$.

Sensing capabilities of nonlinearity-induced BIC. The importance of the above results can be legitimized in the optical domain with several well known systems, including, for instance, Sagnac resonators [56,57] among other settings [40]. The presence of BICs at points $x_\pm$ contributes to the significantly improved sensitivity of the nonlinear response to variations in the system parameters, in particular, to perturbations in the natural frequency of the active nonlinear medium. The remarkable sensitivity is a direct upshot of the existence of first- or second-order poles at $x = x_\pm$ in the first derivative of the nonlinear response, which has the functional form

$$\frac{dx}{d\delta_b} = -\frac{x(x + \tilde{\delta}_R/2)}{3(x - x_-)(x - x_+)}, \tag{21}$$

analogous to Eq. (10). Therefore, it immediately follows that adjacent to the turning points, we have $|\frac{dx}{d\delta_b}| \sim |I(x_\pm) - I|^{-1/2}$. By the same token, close to the inflection point, the sensitivity scales as $|I_c - I|^{-2/3}$.

Sensing in magnetic systems. In view of the extensive studies on nonlinearities [41] in ferrimagnetic spheres, it is worthwhile to consider magnetic systems to implement the sensing scheme. Note that the anharmonicities in optical systems are a direct consequence of the nonlinear response of electrical polarization. In stark contrast, the anharmonic component in a magnetic system originates from the nonlinear magnetization. We consider a single ferromagnetic yttrium iron garnet (YIG) interacting with a microwave cavity as portrayed in Fig. 3. The ferromagnet couples strongly with the microwave field at room temperature, giving rise to quasiparticles, namely cavity-magnon polaritons. The YIG acts as an active Kerr medium, which can be pinned down to the magnetocrystalline anisotropy [41,42,58] of the sample. A strong microwave pump of power P_d and frequency ω_d is used to stimulate the weak anharmonicity of the YIG, which is of the order 10^{-9} Hz. The full Hamiltonian of the cavity-magnon system is consistent with Eq. (11), where the mode operators a, b are respectively superseded by cavity and magnon annihilation operators. The quantities ω_a and ω_b represent the cavity and Kittel mode resonance frequencies. The Rabi frequency of external pumping takes the form $\Omega = \gamma_e \sqrt{\frac{5\pi\rho d P_d}{3c}}$, where γ_e is the gyromagnetic ratio, ρ denotes the spin density of the YIG with a diameter d, and c stands for the velocity of light. For experimentally realizable parameters, we plot in

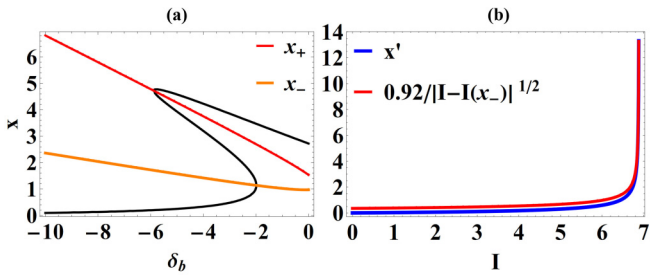

FIG. 4. (a) The δ_b-x curve for $I = 18$ (black line) and the turning points $x_\pm$ plotted against δ_b (red line and orange line, respectively). (b) $x' = \frac{dx}{d\delta_b}$ and $0.92/|I - I(x_-)|^{1/2}$ are plotted against I to make a comparison when $\delta_b = 0$. Parameters are $\gamma_a = \gamma_b = 1$, $g = \delta_a = 4$.

Fig. 4 values of the output intensity x [from Eq. (13)] and remarkable sensing capability x'. Note that currently the study of YIG systems is in vogue, and hence such systems would be a natural choice to study nonlinearity-induced BIC [58,59].

V. CONCLUSIONS

In conclusion, we have demonstrated a new scheme apropos of single- and two-mode Kerr nonlinear systems to engineer BICs. In the context of single-mode systems, we considered a passive Kerr nonlinearity in an optical cavity that demonstrates bistability. As the the system parameters are tuned in close proximity to the turning points of the hysteresis, a BIC springs into existence marked by a vanishing linewidth of the mode. In the neighborhood of the BIC, the steady state response was observed to show pronounced sensitivity to perturbations in the detunings. This remarkable sensitivity can be traced down to the existence of poles in the first-order derivative of the response with respect to the perturbation variable. The sensitivity to perturbations scales as inverse square root of the deviations in external pump powers optimal for the turning points. Further, we extended the analysis into the regime of two-mode systems possessing an active nonlinear medium. Our analysis is generic, applicable to a large class of systems, including, both optical and magnetic systems. Some of the passive nonlinear optical platforms include nonlinear media like CS_2, nitrobenzene, and Rb vapor, whereas high-quality Sagnac resonators support active Kerr nonlinearities. In addition, we considered an active Kerr medium provided by magnetic systems interacting with a microwave cavity where research activity has flourished of late. In the domain of large detunings of the active Kerr medium, the two-mode setup can be described by an effectively single-mode anharmonic system in lock step with the results from the passive Kerr nonlinearity in an optical cavity.

ACKNOWLEDGMENTS

The authors acknowledge the support of the Air Force Office of Scientific Research (AFOSR Award No. FA9550-20-1-0366), the Robert A. Welch Foundation (Grant No. A-1943), and the Herman F. Heep and Minnie Belle Heep Texas A&M University endowed fund.

Q.M. and J.M.P.N. contributed equally to this work.

APPENDIX: EQUIVALENCE BETWEEN SINGLE-MODE AND TWO-MODE ANHARMONIC SYSTEMS

So far, we have discussed schemes for the creation of BICs in single- and two-mode nonlinear systems. It is worth mentioning that there exists a close correspondence between the two-mode and single-mode results in the limit of large δ_b. To enunciate this, let us delve into the second part of Eq. (12). In the long-time limit, we have

$$-(i\delta_b + \gamma_b)m - 2iUb^\dagger bb - iga + \Omega = 0. \tag{A1}$$

Note that the effect of γ_b pales in comparison with δ_b, and we can recast the above equation into

$$b = -\frac{(ga + i\Omega)}{\delta_b}[1 + x]^{-1}, \tag{A2}$$

where $x = \frac{2U|b|^2}{\delta_b}$. For the purpose of simplification, we set $\Omega = 0$ and assume that the external drive is on the cavity at Rabi frequency $\mathcal{E}$. Owing to the largeness of δ_b, it is discernible that $x \ll 1$. Therefore, we can revise the above equation as

$$b = -\frac{(ga + i\Omega)}{\delta_b}[1 - x + O(x^2)]. \tag{A3}$$

Keeping only terms up to first order in x, we are left with $b = -\frac{ga}{\delta_b}[1 - \frac{2U|b|^2}{\delta_b}]$. Upon iterating the solution and omitting the higher order terms, the approximate solution for b transforms into

$$b = -\frac{ga}{\delta_b} + 2\left(\frac{g}{\delta_b}\right)^3\left(\frac{U}{\delta_b}\right)|a|^2 a. \tag{A4}$$

Substituting this into the first part of Eq. (12), we obtain an effective single mode description of the dynamics of the system,

$$\dot{a} = -(i\tilde{\delta}_a + \gamma_a)a - i\tilde{U}|a|^2 a + \mathcal{E}, \tag{A5}$$

where $\tilde{\delta}_a = \delta_a - \frac{g^2}{\delta_a}$ and $\tilde{U} = 2(\frac{g}{\delta_b})^4 U$. Strikingly, the preceding equation reproduces Eq. (3) with Δ, γ, and $2U$ respectively replaced by $\tilde{\delta}_a$, γ_a, and $\tilde{U}$, unfolding the equivalence between two-mode and single-mode nonlinear systems in the realm of large δ_b.

[1] C. W. Hsu, B. Zhen, A. D. Stone, J. D. Joannopoulos, and M. Soljačić, Bound states in the continuum, Nat. Rev. Mater. **1**, 16048 (2016).

[2] J. Von Neumann and E. Wigner, On some peculiar discrete eigenvalues, Phys. Z **30**, 465 (1929).

[3] F. H. Stillinger and D. R. Herrick, Bound states in the continuum, Phys. Rev. A **11**, 446 (1975).

[4] F. Capasso, C. Sirtori, J. Faist, D. L. Sivco, S.-N. G. Chu, and A. Y. Cho, Observation of an electronic bound state above a potential well, Nature (London) **358**, 565 (1992).

[5] A. Albo, D. Fekete, and G. Bahir, Electronic bound states in the continuum above (Ga,In)(As,N)/(Al,Ga)As quantum wells, Phys. Rev. B **85**, 115307 (2012).

[6] C. Álvarez, F. Domínguez-Adame, P. Orellana, and E. Díaz, Impact of electron–vibron interaction on the bound states in the continuum, Phys. Lett. A **379**, 1062 (2015).

[7] J.-X. Yan and H.-H. Fu, Bound states in the continuum and fano antiresonance in electronic transport through a four-quantum-dot system, Phys. B: Condens. Matter **410**, 197 (2013).

[8] A. Lyapina, D. Maksimov, A. Pilipchuk, and A. Sadreev, Bound states in the continuum in open acoustic resonators, J. Fluid Mech. **780**, 370 (2015).

[9] Y. Chen, Z. Shen, X. Xiong, C.-H. Dong, C.-L. Zou, and G.-C. Guo, Mechanical bound state in the continuum for optomechanical microresonators, New J. Phys. **18**, 063031 (2016).

[10] S. Hein, W. Koch, and L. Nannen, Trapped modes and fano resonances in two-dimensional acoustical duct–cavity systems, J. Fluid Mech. **692**, 257 (2012).

[11] D. C. Marinica, A. G. Borisov, and S. V. Shabanov, Bound states in the continuum in photonics, Phys. Rev. Lett. **100**, 183902 (2008).

[12] C.-L. Zou, J.-M. Cui, F.-W. Sun, X. Xiong, X.-B. Zou, Z.-F. Han, and G.-C. Guo, Guiding light through optical bound states in the continuum for ultrahigh-Q microresonators, Laser Photonics Rev. **9**, 114 (2015).

[13] Z. Yu, X. Xi, J. Ma, H. K. Tsang, C.-L. Zou, and X. Sun, Photonic integrated circuits with bound states in the continuum, Optica **6**, 1342 (2019).

[14] Z. Yu, Y. Tong, H. K. Tsang, and X. Sun, High-dimensional communication on etchless lithium niobate platform with photonic bound states in the continuum, Nat. Commun. **11**, 2602 (2020).

[15] A. Kodigala, T. Lepetit, Q. Gu, B. Bahari, Y. Fainman, and B. Kanté, Lasing action from photonic bound states in continuum, Nature (London) **541**, 196 (2017).

[16] C. M. Gentry and M. A. Popović, Dark state lasers, Opt. Lett. **39**, 4136 (2014).

[17] B. Midya and V. V. Konotop, Coherent-perfect-absorber and laser for bound states in a continuum, Opt. Lett. **43**, 607 (2018).

[18] S. T. Ha, Y. H. Fu, N. K. Emani, Z. Pan, R. M. Bakker, R. Paniagua-Domínguez, and A. I. Kuznetsov, Directional lasing in resonant semiconductor nanoantenna arrays, Nat. Nanotechnol. **13**, 1042 (2018).

[19] M. Wu, S. T. Ha, S. Shendre, E. G. Durmusoglu, W.-K. Koh, D. R. Abujetas, J. A. Sánchez-Gil, R. Paniagua-Domínguez, H. V. Demir, and A. I. Kuznetsov, Room-temperature lasing in colloidal nanoplatelets via mie-resonant bound states in the continuum, Nano Lett. **20**, 6005 (2020).

[20] S. I. Azzam, K. Chaudhuri, A. Lagutchev, Z. Jacob, Y. L. Kim, V. M. Shalaev, A. Boltasseva, and A. V. Kildishev, Single and multi-mode directional lasing from arrays of dielectric nanoresonators, Laser Photonics Rev. **15**, 2000411 (2021).

[21] N. Muhammad, Y. Chen, C.-W. Qiu, and G. P. Wang, Optical bound states in continuum in MoS_2-based metasurface for directional light emission, Nano Lett. **21**, 967 (2021).

[22] J.-H. Yang, Z.-T. Huang, D. N. Maksimov, P. S. Pankin, I. V. Timofeev, K.-B. Hong, H. Li, J.-W. Chen, C.-Y. Hsu, Y.-Y. Liu *et al.*, Low-threshold bound state in the continuum lasers in hybrid lattice resonance metasurfaces, Laser Photonics Rev. **15**, 2100118 (2021).

[23] A. Ndao, L. Hsu, W. Cai, J. Ha, J. Park, R. Contractor, Y. Lo, and B. Kanté, Differentiating and quantifying exosome secretion from a single cell using quasi-bound states in the continuum, Nanophotonics **9**, 1081 (2020).

[24] S. Romano, G. Zito, S. Torino, G. Calafiore, E. Penzo, G. Coppola, S. Cabrini, I. Rendina, and V. Mocella, Label-free sensing of ultralow-weight molecules with all-dielectric metasurfaces supporting bound states in the continuum, Photon. Res. **6**, 726 (2018).

[25] A. Tittl, A. Leitis, M. Liu, F. Yesilkoy, D.-Y. Choi, D. N. Neshev, Y. S. Kivshar, and H. Altug, Imaging-based molecular barcoding with pixelated dielectric metasurfaces, Science **360**, 1105 (2018).

[26] A. Leitis, A. Tittl, M. Liu, B. H. Lee, M. B. Gu, Y. S. Kivshar, and H. Altug, Angle-multiplexed all-dielectric metasurfaces for broadband molecular fingerprint retrieval, Sci. Adv. **5**, eaaw2871 (2019).

[27] B. Zhen, S.-L. Chua, J. Lee, A. W. Rodriguez, X. Liang, S. G. Johnson, J. D. Joannopoulos, M. Soljačić, and O. Shapira, Enabling enhanced emission and low-threshold lasing of organic molecules using special Fano resonances of macroscopic photonic crystals, Proc. Natl. Acad. Sci. USA **110**, 13711 (2013).

[28] T. Sun, S. Kan, G. Marriott, and C. Chang-Hasnain, High-contrast grating resonators for label-free detection of disease biomarkers, Sci. Rep. **6**, 1 (2016).

[29] Y. Wang, M. A. Ali, E. K. Chow, L. Dong, and M. Lu, An optofluidic metasurface for lateral flow-through detection of breast cancer biomarker, Biosens. Bioelectron. **107**, 224 (2018).

[30] Y. Wang, Z. Han, Y. Du, and J. Qin, Ultrasensitive terahertz sensing with high-Q toroidal dipole resonance governed by bound states in the continuum in all-dielectric metasurface, Nanophotonics **10**, 1295 (2021).

[31] F. Yesilkoy, E. R. Arvelo, Y. Jahani, M. Liu, A. Tittl, V. Cevher, Y. Kivshar, and H. Altug, Ultrasensitive hyperspectral imaging and biodetection enabled by dielectric metasurfaces, Nat. Photon. **13**, 390 (2019).

[32] Y. Jahani, E. R. Arvelo, F. Yesilkoy, K. Koshelev, C. Cianciaruso, M. De Palma, Y. Kivshar, and H. Altug, Imaging-based spectrometer-less optofluidic biosensors based on dielectric metasurfaces for detecting extracellular vesicles, Nat. Commun. **12**, 3246 (2021).

[33] J. M. Foley, S. M. Young, and J. D. Phillips, Symmetry-protected mode coupling near normal incidence for narrow-band transmission filtering in a dielectric grating, Phys. Rev. B **89**, 165111 (2014).

[34] L. L. Doskolovich, E. A. Bezus, and D. A. Bykov, Integrated flat-top reflection filters operating near bound states in the continuum, Photon. Res. **7**, 1314 (2019).

[35] H. M. Doeleman, F. Monticone, W. den Hollander, A. Alù, and A. F. Koenderink, Experimental observation of a polarization vortex at an optical bound state in the continuum, Nat. Photon. **12**, 397 (2018).

[36] B. Wang, W. Liu, M. Zhao, J. Wang, Y. Zhang, A. Chen, F. Guan, X. Liu, L. Shi, and J. Zi, Generating optical vortex beams by momentum-space polarization vortices centred at bound states in the continuum, Nat. Photon. **14**, 623 (2020).

[37] A. Henkel, M. Meudt, M. Buchmüller, and P. Görrn, Electrically switchable broadband photonic bound states in the continuum, arXiv:2102.01686.

[38] K. Koshelev and Y. Kivshar, Dielectric resonant metaphotonics, ACS Photonics **8**, 102 (2021).

[39] L. Carletti, K. Koshelev, C. De Angelis, and Y. Kivshar, Giant nonlinear response at the nanoscale driven by bound states in the continuum, Phys. Rev. Lett. **121**, 033903 (2018).

[40] R. W. Boyd, *Nonlinear Optics* (Academic, New York, 2020).

[41] Y.-P. Wang, G.-Q. Zhang, D. Zhang, X.-Q. Luo, W. Xiong, S.-P. Wang, T.-F. Li, C.-M. Hu, and J. Q. You, Magnon Kerr effect in a strongly coupled cavity-magnon system, Phys. Rev. B **94**, 224410 (2016).

[42] R.-C. Shen, Y.-P. Wang, J. Li, S.-Y. Zhu, G. S. Agarwal, and J. Q. You, Long-time memory and ternary logic gate using a multistable cavity magnonic system, Phys. Rev. Lett. **127**, 183202 (2021).

[43] J. M. P. Nair, D. Mukhopadhyay, and G. S. Agarwal, Enhanced sensing of weak anharmonicities through coherences in dissipatively coupled anti-PT symmetric systems, Phys. Rev. Lett. **126**, 180401 (2021).

[44] M. Yu, H. Shen, and J. Li, Magnetostrictively induced stationary entanglement between two microwave fields, Phys. Rev. Lett. **124**, 213604 (2020).

[45] J. M. P. Nair, D. Mukhopadhyay, and G. S. Agarwal, Ultralow threshold bistability and generation of long-lived mode in a dissipatively coupled nonlinear system: Application to magnonics, Phys. Rev. B **103**, 224401 (2021).

[46] W. Chen, Ş. Kaya Özdemir, G. Zhao, J. Wiersig, and L. Yang, Exceptional points enhance sensing in an optical microcavity, Nature (London) **548**, 192 (2017).

[47] H. Hodaei, A. U. Hassan, S. Wittek, H. Garcia-Gracia, R. El-Ganainy, D. N. Christodoulides, and M. Khajavikhan, Enhanced sensitivity at higher-order exceptional points, Nature (London) **548**, 187 (2017).

[48] C. E. Rüter, K. G. Makris, R. El-Ganainy, D. N. Christodoulides, M. Segev, and D. Kip, Observation of parity–time symmetry in optics, Nat. Phys. **6**, 192 (2010).

[49] D. Mukhopadhyay, J. M. P. Nair, and G. S. Agarwal, Anti-$\mathcal{PT}$ symmetry enhanced interconversion between microwave and optical fields, Phys. Rev. B **105**, 064405 (2022).

[50] Y.-P. Wang, J. W. Rao, Y. Yang, P.-C. Xu, Y. S. Gui, B. M. Yao, J. Q. You, and C.-M. Hu, Nonreciprocity and unidirectional invisibility in cavity magnonics, Phys. Rev. Lett. **123**, 127202 (2019).

[51] D. Mukhopadhyay and G. S. Agarwal, Multiple Fano interferences due to waveguide-mediated phase coupling between atoms, Phys. Rev. A **100**, 013812 (2019).

[52] L. Lugiato, F. Prati, and M. Brambilla, *Nonlinear Optical Systems* (Cambridge University Press, Cambridge, 2015).

[53] H. M. Gibbs, S. L. McCall, and T. N. C. Venkatesan, Differential gain and bistability using a sodium-filled Fabry-Perot interferometer, Phys. Rev. Lett. **36**, 1135 (1976).

[54] T. Venkatesan and S. McCall, Optical bistability and differential gain between 85 and 296 °K in a Fabry-Perot containing ruby, Appl. Phys. Lett. **30**, 282 (1977).

[55] H. Gibbs, *Optical Bistability: Controlling Light with Light* (Elsevier, Amsterdam, 2012).

[56] H. Zhang, R. Huang, S.-D. Zhang, Y. Li, C.-W. Qiu, F. Nori, and H. Jing, Breaking anti-*PT* symmetry by spinning a resonator, Nano Lett. **20**, 7594 (2020).

[57] J. M. Silver, L. Del Bino, M. T. Woodley, G. N. Ghalanos, A. Ø. Svela, N. Moroney, S. Zhang, K. T. Grattan, and P. Del'Haye, Nonlinear enhanced microresonator gyroscope, Optica **8**, 1219 (2021).

[58] Y.-P. Wang, G.-Q. Zhang, D. Zhang, T.-F. Li, C.-M. Hu, and J. Q. You, Bistability of cavity magnon polaritons, Phys. Rev. Lett. **120**, 057202 (2018).

[59] R.-C. Shen, J. Li, Z.-Y. Fan, Y.-P. Wang, and J. Q. You, Mechanical bistability in Kerr-modified cavity magnomechanics, Phys. Rev. Lett. **129**, 123601 (2022).